

Real-Time Source Independent Quantum Random Number Generator with Squeezed States

Thibault Michel,^{1,2,*} Jing Yan Haw,¹ Davide G. Marangon,³ Oliver Thearle,¹ Giuseppe Vallone,^{3,4} Paolo Villoresi,^{3,4} Ping Koy Lam,^{1,†} and Syed M. Assad¹

¹*Center for Quantum Computation and Communication Technology, Department of Quantum Science, The Australian National University, Canberra, ACT 0200, Australia*

²*Laboratoire Kastler Brossel, UPMC-Sorbonne Universités, CNRS,*

ENS-PSL Research University, Collège de France, 4 place Jussieu, 75252 Paris, France

³*Dipartimento di Ingegneria dell'Informazione, Università degli Studi di Padova, Via Gradenigo 6B, 35131 Padova, Italy*

⁴*Istituto di Fotonica e Nanotecnologie —CNR, Via Trasea 7, 35131 Padova, Italy*

Random numbers are a fundamental ingredient for many applications including simulation, modelling and cryptography. Sound random numbers should be independent and uniformly distributed. Moreover, for cryptographic applications they should also be unpredictable. We demonstrate a real-time self-testing source independent quantum random number generator (QRNG) that uses squeezed light as source. We generate secure random numbers by measuring the quadratures of the electromagnetic field without making any assumptions on the source; only the detection device is trusted. We use a homodyne detection to alternatively measure the \hat{Q} and \hat{P} conjugate quadratures of our source. Using the entropic uncertainty relation, measurements on \hat{P} allows us to estimate a bound on the min-entropy of \hat{Q} conditioned on any classical or quantum side information that a malicious eavesdropper may detain. This bound gives the minimum number of secure bits we can extract from the \hat{Q} measurement. We discuss the performance of different estimators for this bound. We operate this QRNG with a squeezed state and we compare its performance with a QRNG using thermal states. The real-time bit rate was 8.2 kb/s when using the squeezed source and between 5.2–7.2 kb/s when the thermal state source was used.

I. INTRODUCTION

Random numbers are used as a resource for many application such as statistical analysis, numerical simulation, encryption and communication protocols. Random numbers must satisfy three main requirements: they must be uniformly distributed, independent and unpredictable. Pseudo random numbers are generated with a computer via algorithmic routines from a seed. They have the advantage of being easy to implement and fast, but they are intrinsically not secure due to their deterministic generation [1] and some commonly used pseudo random number generators (PRNG) have been shown to be insecure [2]. Their randomness can also be flawed [3] which can lead to errors in simulations [4, 5]. Physical random number generators use a stochastic physical process as the source of randomness [6, 7]. They are slower than PRNGs but can still achieve very high generation rate and has been used as a seed for PRNGs. For random number generators based on classical systems, the randomness usually originate as lack of knowledge on the initial state of the system, in which case the security relies on the assumption that no one has a better knowledge of this original state. Quantum systems on the other hand [8] offer an interesting alternative source of randomness as measurement outcomes on such systems are intrinsically random due to Born's rule [9]. It

is then possible to create a long-term stable [10], fast quantum random number generator (QRNG) [11–13], in a self testing fashion [14], or even on a mobile phone [15]. However the measurement outcomes may still be correlated with another party [16]. This is the case whenever the source of randomness is in a mixed state. Even in that case, it is still possible to exploit non-local Bell state measurement [17, 18] to extract true random numbers without any assumption on the source of randomness or the measurement device [19–23]. However these implementation are still very slow with rates around few tens of bits per second. In a similar fashion, generation protocols using light emitted from distant cosmic sources were recently proposed and demonstrated [24–26]. As a faster alternative one can implement a semi device independent QRNG by assuming only either the source [27] or the detection [28–32] device is trusted. In a source independent quantum random number generator (SI-QRNG), the source of randomness can be arbitrary and controlled by an adversarial party; yet it can still yield secure random numbers. Roughly speaking, the principle of SI-QRNG is that, by switching between different measurement basis, one is able to assess the purity of the source, which can in turn set a bound on its extractable randomness. This can be formalized rigorously using the entropic uncertainty relation [33] which was first introduced in [34].

SI-QRNG based on the entropic uncertainty relation have already been demonstrated in both discrete [28] and continuous variables [30]. However, in these proof of principle experiments, the randomness estimation was always evaluated in post processing after collecting all

* thibault.michel@lkb.upmc.fr

† ping.lam@anu.edu.au

the raw data. Here we implement a continuous variable SI-QRNG where all processing is done in real-time. Additionally, we dynamically switch between two measurement basis to alternate between a *check measurement* and a *random-data measurement*. The SI-QRNG is self testing and changes its output secure bit rate depending on the check measurement data. Although theoretical proposal for using squeezed states as sources of entropy for a QRNG have been suggested [30, 35], we report the first experimental use of squeezed states as an entropy source for a QRNG.

The paper is organized as follows. In section II we present the protocol and experimental details for generating random numbers. The protocol requires estimating a lower bound to the conditional min-entropy. In section III, we present the real-time entropy estimation procedure and the statistics of the random numbers generated. Due to finite sample size, we find that the evaluated conditional min-entropy is positively biased which can lead to an overestimation of the randomness rate. To mitigate this, we propose and discuss other more robust estimators in section IV. Finally, we conclude in section V with a discussion of several ways for extending the work in this paper as well as a summary of our work.

II. PROTOCOL AND EXPERIMENT

In a SI-QRNG, we are attempting to generate secure random numbers without having to trust the source state. This is possible by performing trusted measurements on two non-commuting observables. Our experiment was performed on continuous variable light fields, and the observables measured are the field quadratures \hat{Q} and \hat{P} . By measuring the check quadrature \hat{P} , we put a bound on how much secure randomness can be extracted on the orthogonal random-data quadrature \hat{Q} . In the following, we provide the details on how a bound on the random-data measurements can be calculated.

A. Randomness bound from conditional min-entropy

In our experiment, even though the quadrature observable has a continuous degree of freedom, the data that is recorded is ultimately discrete. The discretization size is determined by the finite resolution of the digitizer. This finite resolution implies that we do not measure the observables \hat{Q} and \hat{P} , but rather their discretized counterparts. Formally we measure a subsection of the positive-operator valued measures (POVM) $\{\hat{Q}_{\delta q}^k\}$ corresponding to $k \in [-\frac{m}{2}, \frac{m}{2} - 1]$, where $\hat{Q}_{\delta q}^k = \int_{I_{\delta q}^k} dq |q\rangle \langle q|$ and

$$I_{\delta q}^k = \begin{cases} (-\infty, (k + \frac{1}{2})\delta q) & \text{for } k = -\frac{m}{2} \\ [(k - \frac{1}{2})\delta q, (k + \frac{1}{2})\delta q) & \text{for } -\frac{m}{2} < k < \frac{m}{2} - 1 \\ [(k - \frac{1}{2})\delta q, \infty) & \text{for } k = \frac{m}{2} - 1. \end{cases}$$

The even integer m denotes the total number of bins, the index k enumerates the outcomes and $\delta q > 0$ specifies the precision of the measurement. The measurement outcomes q_k on state ρ_A , appear with probability $\mathbf{p}(q_k) = \text{Tr}[\rho_A \hat{Q}_{\delta q}^k]$ and are stored in a classical register $Q_{\delta q}$.

When measuring the discretized quadrature $\hat{Q}_{\delta q}$, the maximum amount of secure extractable randomness from a single shot measurement of $Q_{\delta q}$ on a state ρ is given by [16, 36–40]

$$r_{\text{sec}}^\epsilon(Q_{\delta q}|E)_\rho = H_{\min}(Q_{\delta q}|E)_\rho - 2 \log_2 \frac{1}{\epsilon}, \quad (1)$$

where ϵ is the security parameter and $H_{\min}(Q_{\delta q}|E)$ is the conditional min-entropy of $Q_{\delta q}$ [41]. The protocol is then said to be ϵ -secure, which means that the probability of distinguishing the output from a truly uniform independent distribution is smaller than $\frac{1}{2}(1+\epsilon)$ [40]. The conditional min-entropy $H_{\min}(Q_{\delta q}|E)$ is defined as [37, 38, 42]

$$H_{\min}(Q_{\delta q}|E)_{\rho_{QE}} = -\log_2 \max_{\{\hat{E}_k\}} \underbrace{\sum_k \mathbf{p}(q_k) \text{Tr}[\hat{E}_k \rho_E^k]}_{p_{\text{guess}}(\{\hat{E}_k\})}, \quad (2)$$

where $\rho_{QE} = \sum_k \mathbf{p}(q_k) |k\rangle_A \langle k| \otimes \rho_E^k$ is the collective classical-quantum state after measurement on system A . ρ_E^k is the state of system E conditioned on measurement k by A , and $\{\hat{E}_k\}$ is a POVM on system E . The quantity $p_{\text{guess}}(\{\hat{E}_k\})$ is the average probability for an adversary Eve to correctly guess the index k using a measurement strategy $\{\hat{E}_k\}$. The maximization on the POVM $\{\hat{E}_k\}$ corresponds to finding the best measurement strategy Eve might apply to guess the index k on the post-measurement state ρ_{QE} . The amount of secure randomness is then the smallest conditional min-entropy for states ρ_{QE} consistent with Alice's state ρ_A . If the state ρ_A is pure, this implies that A and E are independent: $\rho_{AE} = \rho_A \otimes \rho_E$, in which case the conditional min-entropy reduces to the classical unconditioned min-entropy

$$H_{\min}(Q_{\delta q}) = -\log_2 \max_k \{\mathbf{p}(q_k)\}. \quad (3)$$

Here Eve's best guessing strategy is to guess the most likely index k everytime. For any state, $H_{\min}(Q_{\delta q}) \geq H_{\min}(Q_{\delta q}|E)$ and the difference can be seen as the amount of side information detained by Eve. To compute the exact value of $H_{\min}(Q_{\delta q}|E)_{\rho_{QE}}$ in (2), one needs to know ρ_{QE} . Since Alice does not have access to E , she would need to perform a complete tomography of ρ_A to find all compatible states ρ_{QE} . This is tedious for an infinite dimensional system. Instead, one can bound $H_{\min}(Q_{\delta q}|E)$ by the max-entropy of the conjugate quadrature $H_{\max}(P_{\delta p})$ using the *entropic uncertainty relation* (EUR) [33, 34, 43–48]. This leads to a lower bound H_{low} :

$$H_{\min}(Q_{\delta q}|E) \geq H_{\text{low}}(P_{\delta p}) := -H_{\max}(P_{\delta p}) - \log_2 c(\delta q, \delta p) \quad (4)$$

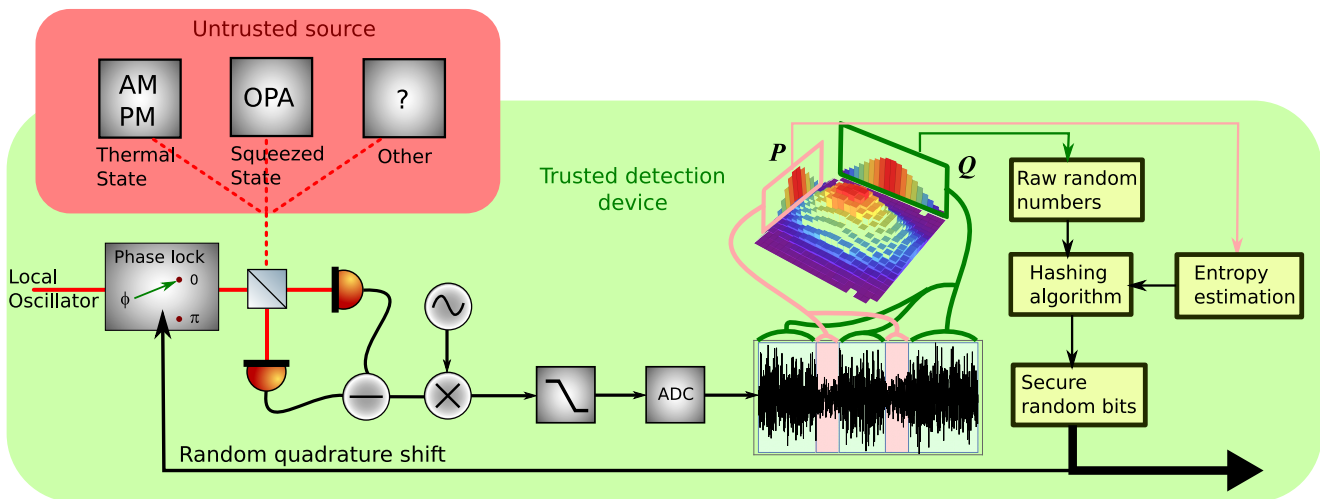


Figure 1: Scheme and protocol of the SI-QRNG. A local oscillator whose phase is locked to measure the *check* quadrature is interfered with an untrusted entropy source which can be a squeezed, thermal or some unknown state. The two output beams are detected and the resulting photocurrents are subtracted. From this homodyne measurement, the min-entropy on the *random-data* quadrature is estimated. The phase lock then switches to the orthogonal random-data quadrature and the same homodyne measurement is performed. The raw random numbers are hashed according to the previous min-entropy estimation. Some of the secure random bits obtained in this way are used to determine when the next lock switch will happen. The check quadrature is measured randomly and on average once every ten runs.

where the max entropy is defined as

$$H_{\max}(P_{\delta p}) = 2 \log_2 \sum_k \sqrt{p(p_k)}. \quad (5)$$

The classical unconditioned max and min entropies are equivalent to the Rényi entropies [49] of order $\frac{1}{2}$ and ∞ respectively. Additionally,

$$c(\delta q, \delta p) = \frac{1}{4\pi} \delta q \delta p S_0^{(1)} \left(1, \frac{\delta q \delta p}{8} \right)^2 \quad (6)$$

is a measure of the incompatibility between the two measurements and $S_0^{(1)}$ is the 0th radial prolate spheroidal wave function of the first kind [50]. This wavefunction comes about by considering the maximum overlap between the eigenstates of $\hat{Q}_{\delta q}$ and $\hat{P}_{\delta p}$ and holds for states ρ_A that has no support in the two extreme bins because those extreme bins have width larger than δq . This requirement correspond to bounding the energy of the input state which is a reasonable assumption. This assumption could be verified by including an energy measurement as part of the protocol [51, 52]. In our real-time demonstration, we just limit the excursion of the state by aborting the protocol when one of the extreme bins is populated.

The bound is unconditional; it is a function of $P_{\delta q}$ only and is independent of E . We use the convention where the vacuum state has a quadrature variance of 1. The \hat{P} quadrature is used as the check quadrature that estimates the amount of randomness extractable in the measurement on the conjugate \hat{Q} which is the random-data quadrature.

B. Experimental details

As shown in Fig.1, the experimental set-up has two parts. The first part is an untrusted entropy source which consists of a quantum state ρ_A that may be mixed and correlated to a malicious party E: $\rho_A = \text{Tr}_E(\rho_{AE})$. We operated the device on two sources, a squeezed state and a thermal state. A shot-noise limited 1064 nm Nd:YAG continuous wave laser provides the laser source for this experiment. A portion of the 1064 nm light is frequency doubled to provide a pump field at 532 nm. Both fields undergo spatial and frequency filtering to provide shot-noise limited light at the sideband frequencies above 2 MHz. The thermal state was generated with an amplitude and phase electro-optic modulators on which we send a white noise electronic signal from two independent function generators. By varying the amplitudes of the noise to the modulators, we varied the variance of this thermal state to see the effect on the secure bit rate. The squeezed state with around 3 dB of squeezing was generated with a seeded doubly resonant optical parametric amplifier in a bow-tie geometry. Details on the squeezed state generation can be found in [53].

The second part of the set-up is a trusted measurement device which consists of a homodyne detector that can measure one of two conjugate quadratures \hat{Q} and \hat{P} on the state ρ_A by locking the phase of a local oscillator (LO) using amplitude or phase modulation. The subtracted current is then mixed down and filtered in the 13 to 17 MHz band before being digitized over $m = 2^{12}$ bins. The measurement device switches randomly between two

measurement states: check measurements and random-data measurements. On average, a check measurement was performed once every ten measurement cycles.

In the check measurement state, three measurement steps are performed. In the first step, the LO and signal beams are blocked using servo-controlled beam-blocks and the electronic dark noise is recorded. In the second step, the signal beam is blocked, while the LO is unblocked. This allows us to record the vacuum shot noise. In the third step, both signal and LO beams are unblocked; the LO is locked to \hat{P} and the check data is recorded. The data is then normalized according to the shot noise corrected of dark noise $\sigma_{\text{corrected}}^2 = \frac{\sigma_{\text{measured}}^2}{\sigma_{\text{shot}}^2 - \sigma_{\text{dark}}^2}$. In this way, all electronic noise will be accounted as impurity on ρ_A .

From the check data, we evaluated the probabilities $\mathbf{p}(p_k)$ using the frequentist estimator and $H_{\text{max}}(P_{\delta p})$ using eqn (5). For each evaluation, the bin size δp is recalculated, in units of shot noise, using the corrected shot noise measurement. The corresponding value of $c(\delta q, \delta p)$ is then evaluated using a pre-calculated polynomial approximation. In the experiment, we had an average $\delta q = (14.45 \pm 0.09) \times 10^{-3}$ and $\delta p = (15.56 \pm 0.09) \times 10^{-3}$ for the thermal state and squeezed state run respectively. The bound $H_{\text{low}}(P_{\delta p})$ is then estimated using (4) and stored in the computer for use in the random-data measurement stage.

In the random-data measurement state, both the signal and LO beams are unblocked. The LO phase is locked to \hat{Q} , and the raw data is recorded. It is then normalized according to the shot noise corrected of dark noise taken from the previous check measurement. In order to eliminate Eve's information, we apply the Toeplitz matrix hashing algorithm [54] on the raw data to obtain the secure random data. The length of the Toeplitz matrix is determined by the randomness bound evaluated in check stage. A few bits of the hashed random numbers are used to determine whether the next stage will be a check or random-data measurement stage.

For both check and random-data measurements, the number of measurements points collected was $n = 16000$. In our implementation, to avoid slowing down the protocol, the random Toeplitz matrix was generated once at the start of the experiment using a trusted QRNG [12] source. However, for the hashing to be fully secure, a new hashing function randomly chosen from a family of two-universal hashing functions should be used every time [40, 55, 56]. This is so that Eve does not have knowledge of the hash function prior to preparing the state such that she cannot implement deception strategies tailored to the hashing function. For monitoring purposes, we also evaluated $H_{\text{min}}(Q_{\delta q})$ using the frequentist estimator. We also check that the homodyne detection was never saturated. If a saturation event is ever detected, the protocol will abort immediately.

III. RESULTS AND ESTIMATION ERROR ANALYSIS

As mentioned before, the QRNG was operated with two different sources; a \hat{P} -squeezed state and a thermal state. In order to generate secure randomness, we use the bound provided by $H_{\text{low}}(P_{\delta p})$ in eq (4). In order to apply this bound, we need to know the value of $H_{\text{max}}(P_{\delta p})$. In subsection III A, we present the real-time experimental result where the frequentist estimator for $H_{\text{max}}(P_{\delta p})$ was used. In subsection III B, we show that this estimator is biased which may compromise the security of the QRNG.

A. Real time entropy estimation

In the experiment, the entropies are calculated in real time using the frequentists estimator. After measuring $n = 16000$ data points, and binning the outcomes into m bins, the frequentist estimators are given by

$$H_{\text{min}}^{\text{freq}}(\vec{n}) = -\log_2 \frac{\max_k \{n_k\}}{n}, \quad (7)$$

$$H_{\text{max}}^{\text{freq}}(\vec{n}) = 2 \log_2 \sum_{k=1}^m \sqrt{\frac{n_k}{n}} \quad (8)$$

where n_k denotes the number of outcomes in the k -th bin and $\vec{n} = (n_1, n_2, \dots, n_m)$. The entropy bounds $H_{\text{low}}^{\text{freq}}(P_{\delta p})$ and the unconditioned classical entropy $H_{\text{min}}^{\text{freq}}(Q_{\delta q})$ from the experiments are recorded for thermal and squeezed state and these are presented as the points in Figs. 2a and 2b. In the same figures, we also plot simulation results $H_{\text{low}}^{\text{sim}}(P_{\delta p})$ and $H_{\text{min}}^{\text{sim}}(Q_{\delta q})$ obtained by sampling n points from a perfect Gaussian distribution. These simulations are repeated 1000 times to estimate the mean and standard deviation of the estimated entropy bound. Finally, the theoretical values we would expect for a perfect discretized Gaussian distribution

$$\mathbf{p}(p_k) = \frac{1}{2} \text{erf} \left(\frac{p_k + \frac{\delta p}{2}}{\sqrt{2}\sigma} \right) - \frac{1}{2} \text{erf} \left(\frac{p_k - \frac{\delta p}{2}}{\sqrt{2}\sigma} \right) \quad (9)$$

are plotted as solid lines $H_{\text{low}}^{\text{th}}(P_{\delta p})$ and $H_{\text{min}}^{\text{th}}(Q_{\delta q})$.

For the squeezed state simulation results, the impurity of the squeezed state was accounted for by inferring the amount of loss on the state from the two quadrature variance measurement. This was estimated to be 33%. This is the reason why the min-entropy and the bound are not equal; they can only be equal for a pure state. Figure 2b shows that higher squeezing give rise to more extractable randomness. Indeed, measuring squeezing on one quadrature guarantees increased noise on the conjugate anti-squeezed quadrature. Unlike in the thermal noise case, this noise is not correlated to another system. For example having 5 dB squeezing on the source increases the entropy rate by around 10% compared to vacuum. Therefore using a squeezed state as an entropy

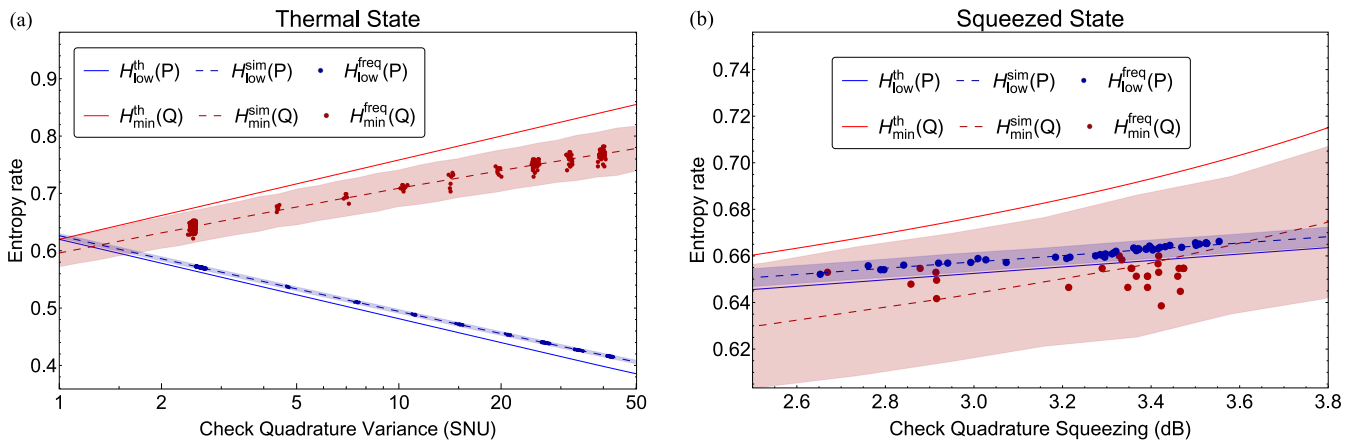


Figure 2: Entropy bound and classical min-entropy for (a) a thermal state with different values of noise and (b) a \hat{P} -squeezed state with 33% loss. The red solid lines show the theoretical unconditioned min entropy of the random-data quadrature \hat{Q} . This gives the extractable randomness if the source is trusted. The blue solid lines show the theoretical bound to the conditional min-entropy $H_{\text{min}}(Q|E)$ obtained by the entropic uncertainty relation. This gives the secure extractable randomness for an untrusted source. The blue and red points show the corresponding experimental data calculated in real-time using a frequentist estimator on data samples of length $n = 16000$. For most values of squeezing, we find that $H_{\text{low}}^{\text{freq}} > H_{\text{min}}^{\text{freq}}$ which would be in violation of the EUR (eqn 4). This apparent violation arises due to a bias in the frequentist estimators. Dashed lines show the corresponding simulation results and the shaded area corresponds to a 5 standard deviation uncertainty region.

source can improve the QRNG bit rate, especially with broadband squeezing. For the squeezed state run the bit rate was 8.2 kb/s.

The thermal state results in Fig. 2a illustrate the difference between the conditioned and unconditioned min-entropy. Indeed a thermal state can be purified by a two-mode squeezed state such that the outcome of a measurement on that state may well be correlated to a mode detained by Eve. This amount of quantum or classical side information is the difference between the min-entropy, which quantifies the entropy of the measurement distribution, and the conditional min-entropy which quantifies the entropy given any possible side information. For a thermal state, the higher the variance the higher the min-entropy which reflects the apparent random noise in quadrature measurement, yet the lower the conditioned min-entropy because the state could be a two-mode squeezed state with higher correlations. For the thermal state run, the bit rate varied between 5.2 kb/s for the state with higher variance to 7.2 kb/s for the state with lower variance.

We tested a collection of random numbers obtained from both the thermal and squeezed states with the NIST statistical test suite [57]. The results are shown in Fig. 3.

B. Bias of the frequentist estimator

We see in Figs. 2a and 2b that there is a discrepancy between the theoretical bound $H_{\text{low}}^{\text{th}}(P_{\delta p})$ and $H_{\text{min}}^{\text{th}}(Q_{\delta q})$ calculated for a Gaussian state and the experimental data. To analyse this we ran a simulation by sampling

a pure Gaussian distribution for different sample size n . Each simulation was repeated 1000 times. As shown in Figs. 4a and 4b, we find that the frequentist estimators $H_{\text{low}}^{\text{freq}}(P_{\delta p})$ and $H_{\text{min}}^{\text{freq}}(Q_{\delta q})$ are both biased. The mean of the frequentist estimators do not match the true values $H_{\text{low}}^{\text{th}}(P_{\delta p})$ and $H_{\text{min}}^{\text{th}}(Q_{\delta q})$. This leads to an apparent violation of the EUR as $H_{\text{low}}^{\text{freq}}(P_{\delta p})$ is positively biased while $H_{\text{min}}^{\text{freq}}(Q_{\delta q})$ is negatively biased. This bias gets smaller as the sample size increases. But even for very large sample size this problem might be present, as it will depend on the source state considered, as shown in Appendix B. Moreover if Eve's state is maximally correlated with ours then any overestimation of the bound will compromise the security of the random numbers. One may try to correct this by using a different estimator for the max-entropy.

IV. OTHER ESTIMATORS FOR THE ENTROPY BOUND

Having learned that the frequentist estimator can be biased, in this section we investigate and compare three different estimators. These estimators comes with their own natural confidence interval that we can set.

A. Bayesian estimator

Another class of possible estimators for H_{max} are the Bayesian estimators. To calculate the Bayes estimator of

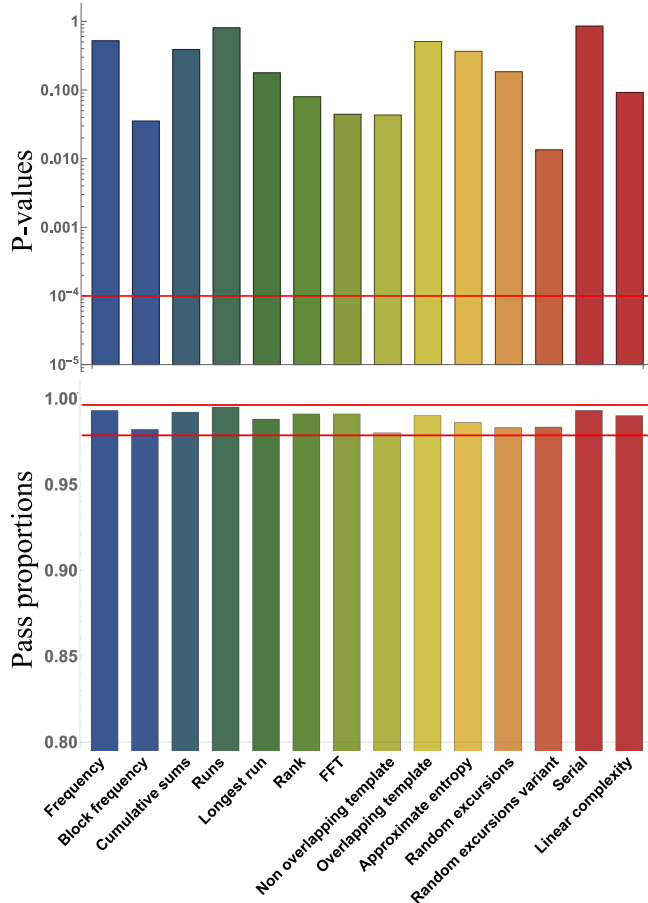


Figure 3: Results of NIST statistical test suites obtained by combining 1000 samples from both the squeezed and thermal state source. Each sample size is 100 kbits and the test significance level is $\alpha = 0.01$. To ‘pass’, the P -values (uniformity of p -values) should be larger than 0.0001 and the pass proportions should be within the Clopper–Pearson interval of $[0.978724, 0.996273]$.

an unknown parameter, one has to specify a prior probability density. This represents our initial belief about the distribution of the unknown parameter. Here we analyse two estimators for H_{\max} based on two different priors. The first is an uninformative prior which makes no assumption on the underlying probability distribution. The second assumes the worst case scenario by choosing a prior peaked around the uniform probability. Deciding which prior to use is a matter of the experimentalist’s degree of paranoia. Even though the QRNG device is source-independent, it is not belief-independent. We note that using Bayesian estimators bring with it the additional advantage of having the posterior estimate as a natural confidence interval.

1. Bayesian estimator for H_{\max} with a completely uninformative prior

The indirect Bayesian estimator with a completely uninformative uniform prior was developed in [58, 59] and proposed for source-device-independent QRNG in [28]. It is given by:

$$H_{\max}^{\text{up}}(\vec{n}) = 2 \log_2 \left(\frac{\Gamma(n+m)}{\Gamma(n+m+\frac{1}{2})} \sum_{k=1}^m \frac{\Gamma(n_k + \frac{3}{2})}{\Gamma(n_k + 1)} \right). \quad (10)$$

Using this estimator in simulation for a gaussian state in our experimental conditions, we find that it has a negative bias which does not lead to a violation of the EUP (see Fig. 5). If one can check that the distribution is Gaussian, it is then justifiable to use the Bayesian estimator. In fact, one can go a step further and remove this bias from the estimator. Otherwise, this negative bias will lead to a severe underestimation of the secure bit rate. But a priori the distribution might not be Gaussian and this bias will depend on the distribution and experimental conditions such as the binning size. We show in Appendix (B) that in some extreme cases this bias can still be positive.

2. Bayesian estimator for H_{\max} with a prior peaked around the uniform distribution

The Bayesian estimator depends on the chosen prior. The natural choice of prior is the Dirichlet distribution since it is the conjugate prior to the multinomial distribution. The Dirichlet distribution parameterised by the vector $\vec{\alpha}$ is given by

$$\text{Dir}[\vec{p}; \vec{\alpha}] = \frac{\Gamma(\sum_{j=1}^m \alpha_j)}{\prod_{j=1}^m \Gamma(\alpha_j)} \prod_{j=1}^m p_j^{\alpha_j - 1},$$

where $\mathbf{p}_j = \mathbf{p}(p_j)$. In order to prevent an underestimation of H_{\max} , it is prudent to assume the worst case scenario by choosing a prior that is sharply peaked around the uniform distribution. This is because the uniform distribution is the distribution with the maximum possible H_{\max} . We subsequently adjust our belief when presented with the measured data. Such a prior can be constructed by choosing $\alpha_j = K$ for all j

$$\pi(\vec{p}) = \text{Dir}[\vec{p}; K] \quad (11)$$

$$= \frac{\Gamma(mK)}{\Gamma(K)^m} (\mathbf{p}_1 \cdots \mathbf{p}_m)^{K-1}. \quad (12)$$

Here K characterize the peakedness of the prior distribution. A large value of K will correspond to a distribution peaked around the uniform distribution, whilst $K = 0$ will correspond to the frequentist estimator. The Bayes posterior estimator given the measurement outcomes \vec{n} is the Dirichlet distribution with parameters $\vec{\alpha} = \vec{n} + K$ [60]

$$f(\vec{p}|\vec{n}) = \text{Dir}[\vec{p}; \vec{n} + K]. \quad (13)$$

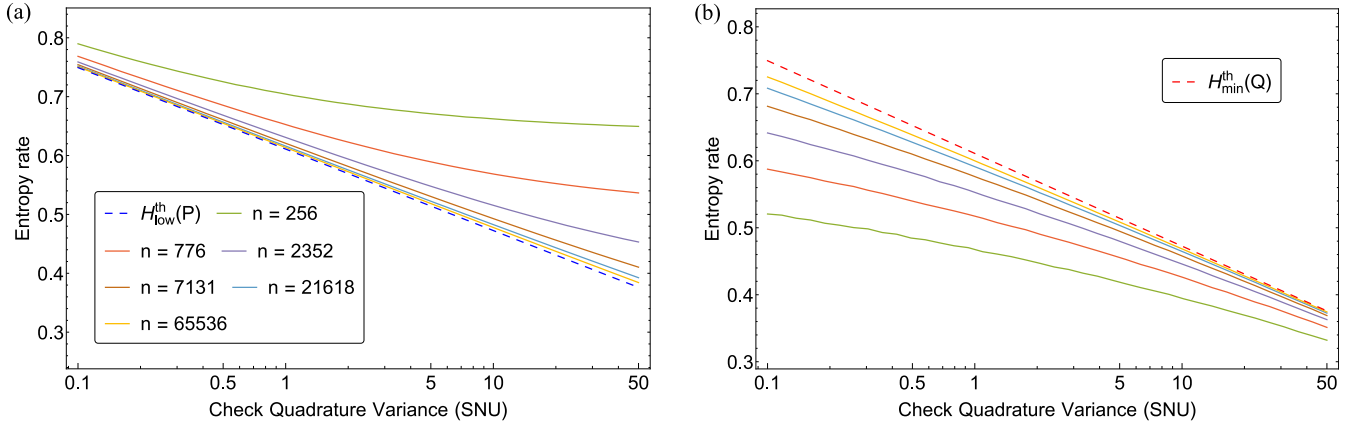


Figure 4: (a) Simulation of the frequentist estimator of the entropy bound for a pure gaussian state. We set $\delta q = 0.0155607$ which was the mean value of δq for the squeezed state runs, and ran the simulation for different sample size. The dashed line shows the theoretical value of $H_{\text{low}}^{\text{th}}$ which gives a lower bound on the conditional min entropy. Due to the finite sample size, the estimator is positively biased which may lead to erroneously extracting more keys than is secure. (b) Simulation of the frequentist estimator of the unconditional min entropy with the same parameters. Due to finite sample size, this estimator is negatively biased which lead to instances where $H_{\text{min}}^{\text{freq}} < H_{\text{low}}^{\text{freq}}$.

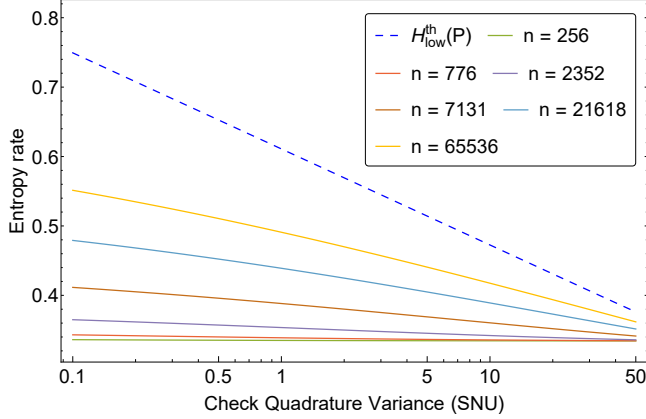


Figure 5: Simulation of the uniform prior Bayesian estimator for the entropy bound of a pure gaussian state with the same parameters as Fig. 4. The estimator is negatively biased which does not compromise security.

From this posterior distribution, we can arrive at a Bayesian estimator for H_{max} . Alternatively, an indirect estimator for H_{max} which we denote by $H_{\text{max}}^{\text{PP}}$ can be obtained by substituting the Bayes posterior mean for the probabilities \vec{p}

$$\mathbf{p}_j^{\text{PP}} = \mathbb{E}[\mathbf{p}_j | \vec{n}] \quad (14)$$

$$= \frac{n_j + K}{n + mK} \quad (15)$$

into (5). As we shall see in section IV C, with a large K , this estimator tends to be very conservative.

B. Extremal Variance-based Estimator

Another way to estimate H_{max} is by estimating the variance distribution. Instead of estimating $H_{\text{max}}(P_{\delta p})$ from the sampled distribution, we can try to bound it. We first estimate V_P , the variance of $P_{\delta p}$ with the unbiased estimator $V_P = \frac{1}{n-1} \sum_{k=1}^n (p_k - \bar{p})^2$. We can then find the distribution that maximizes H_{max} for this given variance. This is similar to the method used in [29] for bounding the Shannon entropy [61, 62].

We show in Appendix A that given a variance V_P , the corresponding extremal distribution is given by

$$\mathbf{p}(p_k) = C \frac{1}{\left(1 + \left(\frac{p_k}{s}\right)^2\right)^2} \quad (16)$$

where

$$C = \sum_j \frac{1}{\left(1 + \left(\frac{p_k}{s}\right)^2\right)^2} \quad (17)$$

is a normalization constant,

$$s = \sqrt{\frac{1 - \gamma V_P}{\gamma}} \quad (18)$$

and γ is the solution to the equation

$$\sum_k \frac{p_k^2 - V_P}{\left(1 + \gamma(p_k^2 - V_P)\right)^2} = 0. \quad (19)$$

This distribution is a discretized Student's t-distribution with 3 degrees of freedom. Although equation (19) does not have a closed form solution for γ , one may calculate it numerically. We can then calculate the extremal variance

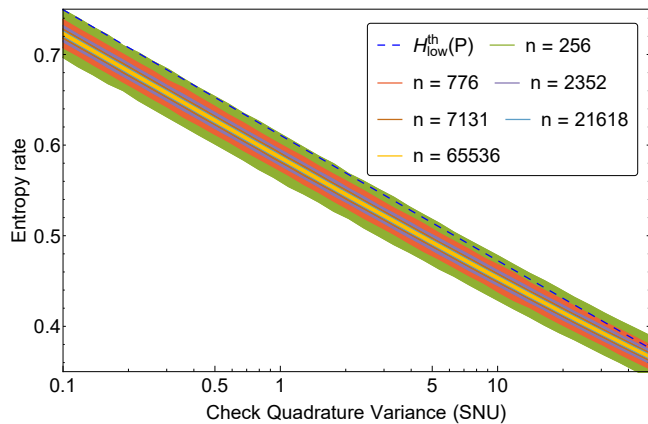


Figure 6: The extremal variance based estimator $H_{\text{low}}^{\text{EVB}}$ obtained by estimating the variance of the check-quadrature. Shaded area shows 5 standard deviation. This estimator shows no bias. The dashed line is the theoretical bound for a Gaussian distribution. The estimator is lower because the extremal distribution for the EVB estimator assumes a discretised Student's t-distribution (eqn 16). For sample size above 1000, the variance of this estimator become small enough so that the probability of a single shot estimation to be above $H_{\text{low}}^{\text{th}}$ becomes negligible.

based (EVB) estimator $H_{\text{max}}^{\text{EVB}}(V_P)$. This is the extremal max-entropy consistent with the variance V_P . From this we get an estimate for $H_{\text{low}}^{\text{EVB}}$ from eqn (4). This is plotted in Fig. 6 for a gaussian state with parameters similar to our experiment.

In these conditions, we see that the EVB estimator shows no bias, the mean value does not change with the sample size. Moreover, by construction, the mean of the EVB estimator for $H_{\text{low}}^{\text{EVB}}$ is always smaller than $H_{\text{low}}^{\text{th}}(P_{\delta p})$. Unlike the frequentist estimators, the EVB estimator does not over-estimate $H_{\text{low}}^{\text{th}}$. However, because the EVB estimator uses only the variance instead of the whole distribution it does not converge to $H_{\text{low}}^{\text{th}}$ even when the sample size is large. It will only converge to $H_{\text{low}}^{\text{th}}$ if the check-quadrature distribution happens to be the discretized Student's t-distribution (16).

We note that here, the theory $H_{\text{low}}^{\text{th}}(P_{\delta p})$ and simulations were computed for Gaussian states. The bias results will differ for other input state and in some cases the EVB estimator can still be positively biased. This is because even though the variance estimator is unbiased, the max-entropy is a concave function of the variance. This means that it will have a negative bias. This is illustrated in Appendix B. However, we can get a confidence interval on the variance from the sampled data and from this we can arrive at a confident estimate for the max-entropy.

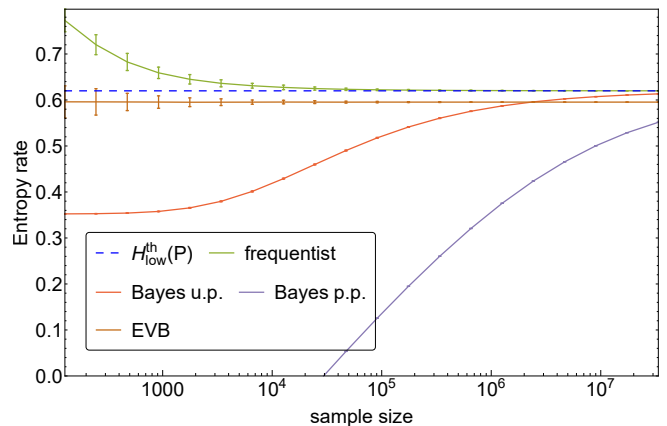


Figure 7: Comparison between frequentist, Bayes and EVB estimators for H_{low} with finite statistics for the vacuum state. For the Bayesian estimator with peaked prior, K was set to 100. Each simulation was repeated 100 times to obtain the estimator mean and standard deviation.

C. Comparison of the different estimator performances

A comparison on how the different estimators perform with increasing sample size for a vacuum state input is shown in Fig. 7. The frequentist estimator has a positive bias leading to an overestimation of the secure randomness rate which can compromise the security of the random numbers. In contrast, the EVB and both Bayes estimators have a negative bias which leads to an underestimation of the secure randomness rate. Of all the estimators, the Bayesian peaked prior estimator is the most conservative, it will significantly underestimate the bound even for large sample sizes.

Finally we note that even with an unbiased estimator for H_{max} , one should not take its mean value as the point estimate. Doing this will lead to a 50% probability of over estimating H_{max} . Instead, one should get a point estimate based on its confidence interval and a required failure rate.

V. CONCLUSION AND OUTLOOK

We demonstrated a real time source independent QRNG incorporating measurement basis switching and hashing using a squeezed state of light as a source of entropy. The protocol was also validated on different thermal states. In the real time demonstration, the sample size was limited by the finite computational resource. A valuable lesson learnt from this demonstration is that due to finite size effects, the frequentist estimator can lead to an underestimation of the max-entropy due to its biased nature. This can lead to an underestimation of the adversary's knowledge on the measured data. To mitigate

this potential problem, we propose three different ways for estimation of the max-entropy. Which one of these estimators the experimenter picks will depend on his level of paranoia.

We note that this estimation problem does not arise in a trusted source QRNG where confidence interval on entropy estimator can be calculated from the knowledge of the source. Nor does it appear in asymptotic CV quantum key distribution (QKD) protocols where the measured distribution can be assumed to be Gaussian due to optimality of Gaussian attacks [63, 64]. For Gaussian distributions, it is then easy to construct a confidence interval for the max-entropy. However, in a source independent protocol, we see that a Gaussian distribution is not the best that the adversary can do. Hence assuming a Gaussian distribution might lead to an underestimation of her knowledge.

The bit rate was limited by three main factors. First, the slow real-time hashing of the raw bits which was done on a desktop computer. Second, the mechanical beam blocking in check measurement. Third, the limited squeezing bandwidth. The first limitation can be circumvented using a fast programmable gate arrays (FPGA) to hash. We foresee that implementing the hashing on an FPGA would allow us to reach the GHz regime [65]. The second limitation is less stringent since the beam blocking only happens during the check-measurement. In our setup, the check-measurement was performed with a 10%

probability and the data-measurement is not limited by these slow mechanical beam blocks. Furthermore, one may use faster, non mechanical ways to block the beam, for example by using acoustic optical modulators to deflect the beams. The third limitation in this experiment was the squeezing bandwidth which is imposed by the bandwidth of the OPA squeezing cavity. Hence, using a squeezed state source may limit the bit rate through bandwidth limitation more than it improves it through the higher security rate. This limitation can be circumvented by using a single pass OPA with would offer squeezing over much larger bandwidths [66].

In conclusion, we demonstrated a real-time source independent maximum bit rate of 8.2 kbits per second with a squeezed state source, and from 5.2 to 7.2 kbits per second with thermal source depending on the variance of the source.

VI. ACKNOWLEDGEMENT

This work was funded by the Australian Research Council Centre of Excellence and Laureate Fellowship schemes (CE110001027 and FL150100019). Our research is also supported by The Defence Industry and Innovation Next Generation Technologies Fund.

We thank Nathan Walk for useful discussions and comments on this work.

-
- [1] P. Hellekalek, *Mathematics and Computers in Simulation* **46**, 485 (1998).
 - [2] Y. Dodis, D. Pointcheval, S. Ruhault, D. Vergniaud, and D. Wichs, *Proceedings of the 2013, ACM SIGSAC conference on Computer and communications security - CCS '13*, 647 (2013).
 - [3] M. Herrero-Collantes and J. C. Garcia-Escartin, *Reviews of Modern Physics* **89** (2017), 10.1103/RevModPhys.89.015004, arXiv: 1604.03304.
 - [4] G. Marsaglia, *Proceedings of the National Academy of Sciences* **61**, 25 (1968).
 - [5] A. M. Ferrenberg, D. P. Landau, and Y. J. Wong, *Physical Review Letters* **69**, 3382 (1992).
 - [6] A. Uchida, K. Amano, M. Inoue, K. Hirano, S. Naito, H. Someya, I. Oowada, T. Kurashige, M. Shiki, S. Yoshimori, K. Yoshimura, and P. Davis, *Nature Photonics* **2**, 728 (2008).
 - [7] D. G. Marangon, G. Vallone, and P. Villoresi, *Scientific Reports* **4** (2015), 10.1038/srep05490.
 - [8] X. Ma, X. Yuan, Z. Cao, B. Qi, and Z. Zhang, *npj Quantum Information* **2** (2016), 10.1038/npjqi.2016.21.
 - [9] J. Rarity, P. Owens, and P. Tapster, *Journal of Modern Optics* **41**, 2435 (1994).
 - [10] D. G. Marangon, A. Plews, M. Lucamarini, J. F. Dynes, A. W. Sharpe, Z. Yuan, and A. J. Shields, *J. Lightwave Technol., JLT* **36**, 3778 (2018).
 - [11] T. Symul, S. M. Assad, and P. K. Lam, *Applied Physics Letters* **98**, 231103 (2011).
 - [12] J. Y. Haw, S. M. Assad, A. M. Lance, N. H. Y. Ng, V. Sharma, P. K. Lam, and T. Symul, *Physical Review Applied* **3** (2015), 10.1103/PhysRevApplied.3.054004, arXiv: 1411.4512.
 - [13] Q. Zhang, X. Deng, C. Tian, and X. Su, *Opt. Lett., OL* **42**, 895 (2017).
 - [14] T. Lunghi, J. B. Brask, C. C. W. Lim, Q. Lavigne, J. Bowles, A. Martin, H. Zbinden, and N. Brunner, *Physical Review Letters* **114** (2015), 10.1103/PhysRevLett.114.150501.
 - [15] B. Sanguinetti, A. Martin, H. Zbinden, and N. Gisin, *Physical Review X* **4** (2014), 10.1103/PhysRevX.4.031056, arXiv: 1405.0435.
 - [16] D. Frauchiger, R. Renner, and M. Troyer, *arXiv:1311.4547 [quant-ph]* (2013), arXiv: 1311.4547.
 - [17] J. S. Bell, *Physics Physique Fizika* **1**, 195 (1964).
 - [18] N. Brunner, D. Cavalcanti, S. Pironio, V. Scarani, and S. Wehner, *Reviews of Modern Physics* **86**, 419 (2014), arXiv: 1303.2849.
 - [19] S. Pironio, A. Acín, S. Massar, A. B. de la Giroday, D. N. Matsukevich, P. Maunz, S. Olmschenk, D. Hayes, L. Luo, T. A. Manning, and C. Monroe, *Nature* **464**, 1021 (2010).
 - [20] B. Christensen, K. McCusker, J. Altepeter, B. Calkins, T. Gerrits, A. E. Lita, A. Miller, L. K. Shalm, Y. Zhang, S. Nam, *et al.*, *Physical review letters* **111**, 130406 (2013).
 - [21] M. Pivoluska, M. Plesch, M. Pivoluskaa, and M. Plesch, *Acta Physica Slovaca* **64**, 601 (2014).
 - [22] Y. Liu, X. Yuan, M.-H. Li, W. Zhang, Q. Zhao, J. Zhong,

- Y. Cao, Y.-H. Li, L.-K. Chen, H. Li, *et al.*, *Physical Review Letters* **120**, 010503 (2018).
- [23] P. Bierhorst, E. Knill, S. Glancy, Y. Zhang, A. Mink, S. Jordan, A. Rommal, Y.-K. Liu, B. Christensen, S. W. Nam, M. J. Stevens, and L. K. Shalm, *Nature* **556**, 223 (2018).
- [24] C. Wu, B. Bai, Y. Liu, X. Zhang, M. Yang, Y. Cao, J. Wang, S. Zhang, H. Zhou, X. Shi, *et al.*, *Physical Review Letters* **118**, 140402 (2017).
- [25] J. Handsteiner, A. S. Friedman, D. Rauch, J. Gallicchio, B. Liu, H. Hosp, J. Kofler, D. Bricher, M. Fink, C. Leung, *et al.*, *Physical Review Letters* **118**, 060401 (2017).
- [26] C. Leung, A. Brown, H. Nguyen, A. S. Friedman, D. I. Kaiser, and J. Gallicchio, *Physical Review A* **97**, 042120 (2018).
- [27] Y.-Q. Nie, J.-Y. Guan, H. Zhou, Q. Zhang, X. Ma, J. Zhang, and J.-W. Pan, *Physical Review A* **94** (2016), 10.1103/PhysRevA.94.060301.
- [28] G. Vallone, D. G. Marangon, M. Tomasin, and P. Villoresi, *Physical Review A* **90** (2014), 10.1103/PhysRevA.90.052327.
- [29] B. Xu, Z. Li, J. Yang, S. Wei, Q. Su, W. Huang, Y. Zhang, and H. Guo, [arXiv:1709.00685 \[quant-ph\]](https://arxiv.org/abs/1709.00685) (2017), [arXiv: 1709.00685](https://arxiv.org/abs/1709.00685).
- [30] D. G. Marangon, G. Vallone, and P. Villoresi, *Physical Review Letters* **118** (2017), 10.1103/PhysRevLett.118.060503, [arXiv: 1509.07390](https://arxiv.org/abs/1509.07390).
- [31] J. Ma, X. Yuan, A. Hakande, and X. Ma, [arXiv:1704.06915 \[quant-ph\]](https://arxiv.org/abs/1704.06915) (2017), [arXiv: 1704.06915](https://arxiv.org/abs/1704.06915).
- [32] M. Avesani, D. G. Marangon, G. Vallone, and P. Villoresi, *Nature Communications* **9** (2018), 10.1038/s41467-018-07585-0.
- [33] F. Furrer, M. Berta, M. Tomamichel, V. B. Scholz, and M. Christandl, *Journal of Mathematical Physics* **55**, 122205 (2014), [arXiv: 1308.4527](https://arxiv.org/abs/1308.4527).
- [34] I. Białynicki-Birula and J. Mycielski, *Communications in Mathematical Physics* **44**, 129 (1975).
- [35] Y. Zhu, G. He, and G. Zeng, *International Journal of Quantum Information* **10**, 1250012 (2012).
- [36] R. Renner, *International Journal of Quantum Information* **6**, 1 (2008).
- [37] R. König, R. Renner, and C. Schaffner, *IEEE Transactions on Information Theory* **55**, 4337 (2009).
- [38] R. König and R. Renner, *IEEE Transactions on Information Theory* **57**, 4760 (2011), [arXiv: 0712.4291](https://arxiv.org/abs/0712.4291).
- [39] M. Tomamichel and M. Hayashi, *IEEE Transactions on Information Theory* **59**, 7693 (2013).
- [40] M. Tomamichel, [arXiv:1504.00233 \[math-ph, physics:quant-ph\]](https://arxiv.org/abs/1504.00233) **5** (2016), 10.1007/978-3-319-21891-5, [arXiv: 1504.00233](https://arxiv.org/abs/1504.00233).
- [41] R. Renner, [arXiv:quant-ph/0512258](https://arxiv.org/abs/quant-ph/0512258) (2005), [arXiv: quant-ph/0512258](https://arxiv.org/abs/quant-ph/0512258).
- [42] M. Tomamichel, R. Colbeck, and R. Renner, *IEEE Transactions on Information Theory* **55**, 5840 (2009), [arXiv: 0811.1221](https://arxiv.org/abs/0811.1221).
- [43] M. Berta, M. Christandl, R. Colbeck, J. M. Renes, and R. Renner, *Nature Physics* **6**, 659 (2010).
- [44] A. E. Rastegin, *Journal of Physics A: Mathematical and Theoretical* **44**, 095303 (2011).
- [45] M. Tomamichel and R. Renner, *Physical Review Letters* **106** (2011), 10.1103/PhysRevLett.106.110506, [arXiv: 1009.2015](https://arxiv.org/abs/1009.2015).
- [46] P. J. Coles, R. Colbeck, L. Yu, and M. Zwoleak, *Physical Review Letters* **108** (2012), 10.1103/PhysRevLett.108.210405.
- [47] J. Zhang, Y. Zhang, and C.-s. Yu, *Quantum Information Processing* **14**, 2239 (2015).
- [48] P. J. Coles, M. Berta, M. Tomamichel, and S. Wehner, *Reviews of Modern Physics* **89** (2017), 10.1103/RevModPhys.89.015002.
- [49] A. Rényi *et al.*, in *Proceedings of the Fourth Berkeley Symposium on Mathematical Statistics and Probability, Volume 1: Contributions to the Theory of Statistics* (The Regents of the University of California, 1961).
- [50] H. J. Landau and H. O. Pollak, *Bell System Technical Journal* **40**, 65 (1961).
- [51] F. Furrer, *Phys. Rev. A* **90**, 042325 (2014).
- [52] Y.-C. Zhang, Z. Chen, C. Weedbrook, S. Yu, and H. Guo, [arXiv:1811.11973 \[quant-ph\]](https://arxiv.org/abs/1811.11973) (2018), [arXiv: 1811.11973](https://arxiv.org/abs/1811.11973).
- [53] H. M. Chrzanowski, S. M. Assad, J. Bernu, B. Hage, A. P. Lund, T. C. Ralph, P. K. Lam, and T. Symul, *Journal of Physics B: Atomic, Molecular and Optical Physics* **46**, 104009 (2013).
- [54] X. Ma, F. Xu, H. Xu, X. Tan, B. Qi, and H.-K. Lo, *Physical Review A* **87** (2013), 10.1103/PhysRevA.87.062327.
- [55] C. H. Bennett, G. Brassard, C. Crépeau, and U. M. Maurer, *IEEE Transactions on Information Theory* **41**, 1915 (1995).
- [56] R. Renner and R. König, in *Theory of Cryptography*, edited by J. Kilian (Springer Berlin Heidelberg, Berlin, Heidelberg, 2005) pp. 407–425.
- [57] A. Rukhin, J. Soto, J. Nechvatal, M. Smid, and E. Barker, *A statistical test suite for random and pseudorandom number generators for cryptographic applications*, Tech. Rep. (Booz-Allen and Hamilton Inc Mclean Va, 2001).
- [58] D. H. Wolpert and D. R. Wolf, *Physical Review E* **52**, 6841 (1995).
- [59] D. Holste, I. Große, and H. Herzog, *Journal of Physics A: Mathematical and General* **31**, 2551 (1998).
- [60] T. Leonard, *Journal of the American Statistical Association* **72**, 869 (1977).
- [61] C. E. Shannon, *BELL SYSTEM TECHNICAL JOURNAL*, 34.
- [62] M. M. Wolf, G. Giedke, and J. I. Cirac, *Physical Review Letters* **96** (2006), 10.1103/PhysRevLett.96.080502.
- [63] R. García-Patrón and N. J. Cerf, *Phys. Rev. Lett.* **97**, 190503 (2006).
- [64] M. Navascués, F. Grosshans, and A. Acín, *Phys. Rev. Lett.* **97**, 190502 (2006).
- [65] X.-G. Zhang, Y.-Q. Nie, H. Zhou, H. Liang, X. Ma, J. Zhang, and J.-W. Pan, *Review of Scientific Instruments* **87**, 076102 (2016).
- [66] S. Ast, M. Mehmet, and R. Schnabel, *Opt. Express, OE* **21**, 13572 (2013).
- [67] O. Johnson and C. Vignat, *Annales de l'Institut Henri Poincaré (B) Probability and Statistics* **43**, 339 (2007).

Appendix A: Extremal distribution for max-entropy with a fixed variance

Suppose we experimentally observed a discrete distribution in a finite support. From the variance of this distribution, we can upper bound its entropy. To do that we shall derive the probability distribution that maximizes the entropy for a fixed variance. We note that entropy does not depend on the labels of the bins; to have a tighter bound we can rearrange the bins to minimize the variance.

Here we derive the probability distribution maximizing max-entropy for a fixed variance in a finite support setting. We want to find the extremal distribution $\mathcal{P} = \{p_k\}$ that maximizes the max entropy:

$$H_{\max}(\vec{p}) = 2 \log_2 \sum_k \sqrt{p_k} \quad (\text{A1})$$

over the finite support $x_k = k \delta x$ for integer values $k \in [-m, m]$ subject to the normalization constraint $\sum_k p_k = 1$ and fixed variance condition:

$$\sum_k p_k x_k^2 - \left(\sum_k p_k x_k \right)^2 = V. \quad (\text{A2})$$

We first show that the extremal distribution must be symmetric with $p_k = p_{-k}$. From an arbitrary distribution $\mathcal{Q} = \{q_k\}$, we can construct a symmetrized distribution $\mathcal{P} = \{p_k\}$ with

$$p_k = \frac{q_k + q_{-k}}{2}.$$

This distribution will have a smaller variance, $\text{var}(\mathcal{P}) \leq \text{var}(\mathcal{Q})$ but higher max entropy $H_{\max}(\mathcal{P}) \geq H_{\max}(\mathcal{Q})$. The first statement holds due to $\langle \mathcal{Q}^2 \rangle = \langle \mathcal{P}^2 \rangle$ and $\langle \mathcal{Q} \rangle^2 \geq \langle \mathcal{P} \rangle^2 = 0$. The second statement follows from the concavity of the entropy function:

$$\begin{aligned} H_{\max}(\mathcal{P}) &= 2 \log_2 \sum_k \sqrt{p_k} \\ &= 2 \log_2 \sum_k \sqrt{\frac{q_k + q_{-k}}{2}} \\ &\geq 2 \log_2 \sum_k \left(\frac{1}{2} \sqrt{q_k} + \frac{1}{2} \sqrt{q_{-k}} \right) \\ &= H_{\max}(\mathcal{Q}). \end{aligned}$$

Hence, the extremal distribution is symmetric and has zero mean.

To find the extremal distribution \mathcal{P} , we write the Lagrangian as:

$$\begin{aligned} L(\mathcal{P}, \alpha, \gamma) &= 2 \log_2 \sum_k \sqrt{p_k} \\ &+ \frac{\alpha}{\ln 2} \left(1 - \sum_k p_k \right) + \frac{\gamma}{\ln 2} \left(V - \sum_k p_k x_k^2 \right). \end{aligned}$$

L attains a stationary point when

$$\begin{aligned} \frac{\partial L}{\partial p_k} &= 0 \\ \Rightarrow \frac{1}{\sqrt{p_k}} \frac{1}{\sum_j \sqrt{p_j}} - \alpha - \gamma x_k^2 &= 0 \\ \Rightarrow \frac{1}{\sqrt{p_k}} &= (\alpha + \gamma x_k^2) \sum_j \sqrt{p_j}. \end{aligned}$$

Multiplying both sides by p_k and summing over k , we obtain the relation:

$$\alpha + \gamma V = 1.$$

This together with the constraint $\frac{\partial L}{\partial \alpha} = 0$ allows us to write

$$p_k = \frac{1}{\sum_j \frac{1}{(1 + \gamma(x_j^2 - V))^2}}.$$

We recognize this as a discretised version of the non-standardized Student's t-distribution with 3 degrees of freedom and standard deviation s :

$$S_3(x; s) = \frac{2}{\pi s \left(1 + \frac{x^2}{s^2} \right)^2}.$$

When $\delta q \rightarrow 0$ and $m \delta q \rightarrow \infty$, we retrieve the continuous limit, $\gamma \rightarrow \frac{1}{2}$ and $s^2 \rightarrow V$. This is consistent with the known result that the Student's t-distribution are the extremal continuous distribution for H_{\max} [67].

A necessary condition for the Lagrange multiplier γ is obtained from the constraint $\frac{\partial L}{\partial \gamma} = 0$ which gives an implicit equation:

$$\begin{aligned} \sum_k \frac{x_k^2}{(1 + \gamma(x_k^2 - V))^2} &= \sum_j \frac{V}{(1 + \gamma(x_j^2 - V))^2} \\ \Rightarrow \sum_k \frac{x_k^2 - V}{(1 + \gamma(x_k^2 - V))^2} &= 0. \end{aligned}$$

Numerically, we see that there can be more than one real solution for γ . The extremal H_{\max} is given by the solution that is closest to zero.

Appendix B: Small number of bins example

In this Appendix, we show that under extreme cases when the number of bins is very small, when the number of samples are very small or when the input state saturates the extreme bins, some of the estimator for H_{\max} proposed in the main text may still be negatively biased, which would lead to a positive bias on H_{low} . To illustrate this we considered three different distributions with only nine bins as shown in Fig. 8. The only estimator that shows no negative bias is the peaked prior Bayes estimator.

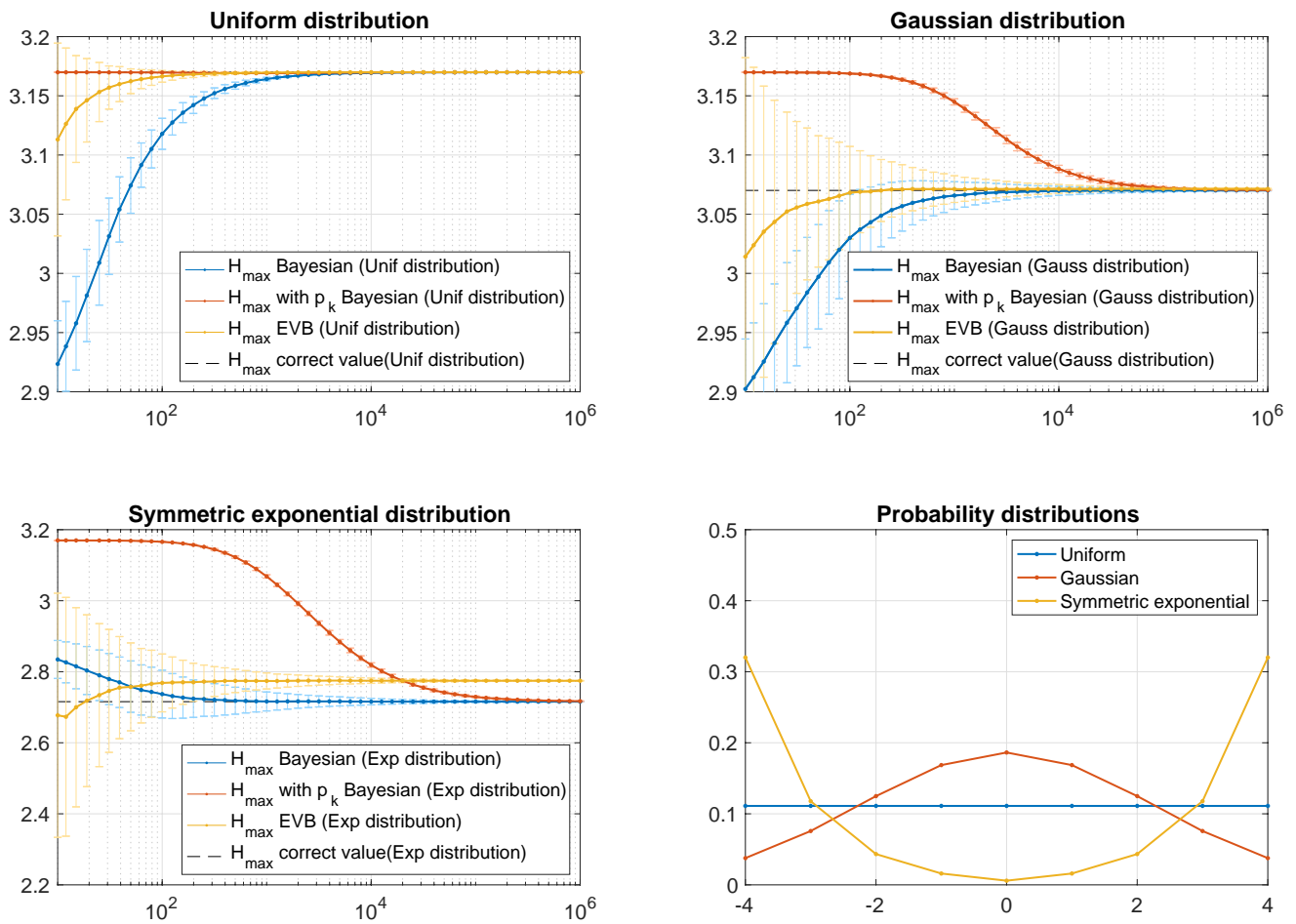


Figure 8: Comparison of estimators for H_{\max} on three probability distributions with just nine bins. A negative bias on H_{\max} translates to a positive bias on H_{low} . For the Bayesian estimator with peaked prior, K was set to 100.